International Journal of Technical Research and Applications e-ISSN: 2320-8163,
www.ijtra.com Volume 2, Issue 1 (jan-feb 2014), PP. 56-72

EVALUATING THICKNESS REQUIREMENTS OF FRACTURE SPECIMEN IN PREDICTING CHARACTERISTIC DISTANCE (LC) USING 3D FEM

Raghvendra Singh, Dr. Sanjeev Saxena, Neha Gupta[#]
Mechanical Department,Babu Banarasi Das University
Lucknow, India
SAMPRI, Habibganj Naka
Bhopal, India

***Abstract*—When a ductile material with a crack is loaded in tension, the deformation energy builds up around the crack tip and it is understood that at a certain critical condition voids are formed ahead of the crack tip. The crack extension occurs by coalescence of voids with the crack tip. The "characteristic distance" (Lc) defined as the distance b/w the crack tip & the void responsible for eventual coalescence with the crack tip. Nucleation of these voids is generally associated with the presence of second phase particles or grain boundaries in the vicinity of the crack tip. Although approximate, Lc assumes a special significance since it links the fracture toughness to the microscopic mechanism considered responsible for ductile fracture. The knowledge of the "characteristic distance" is also crucial for designing the size of mesh in the finite element simulations of material crack growth using damage mechanics principles. There is not much work (experimental as well as numerical) available in the literature related to the dependency of "characteristic distance" on the fracture specimen geometry. The present research work is an attempt to understand numerically, the geometry dependency of "characteristic distance" using three-dimensional FEM analysis. The variation of "characteristic distance" parameter due to the change of temperature across the fracture specimen thickness was also studied. The work also studied the variation of "characteristic distance", due to the change in fracture specimen thickness. Finally, the ASTM requirement of fracture specimen thickness criteria is evaluated for the "characteristic distance" fracture parameter. "Characteristic distance" is found to vary across the fracture specimen thickness. It is dependent on fracture specimen thickness and it converges after a specified thickness of fracture specimen. "Characteristic distance" value is also dependent on the temperature of ductile material. In Armco iron material, it is found to decrease with the increase in temperature.**

***Keywords*— J-integral, CTOD, SIF (K), Energy Release Rate (G), Characteristic Distance (lc)**

I. INTRODUCTION

Now a day modern industry like automobile, aerospace, and power plants are demanding materials to be used under severe conditions. This is required to optimize the design dimensions and cut costs without reducing the safety margins. The material properties are very important to choose right material for the right component or part. The material properties are classified as: Mechanical properties, Electrical properties, Thermal properties, Chemical properties, Magnetic properties, Electrical properties, Atomic properties manufacturing properties etc. While designing these components ductile material is the obvious choice as these material exhibits larger plastic deformation and possesses larger crack initiation and crack growth life in comparison to brittle material. When the ductile material is mechanically stressed it exhibits in a sequence the following three responses: the elastic response, the plastic response and finally the fracture of the material. The study of formation of crack in materials comes under the field of fracture mechanics. Fracture mechanics is based on the implicit assumption that there exists a crack in the structural component.

Fracture mechanics deals with the question-whether a known crack is likely to grow under a certain given loading condition or not. When a material with a crack is loaded in tension, the deformation energy builds up around the crack tip and it is understood that at a certain critical condition voids are formed ahead of the crack tip. The crack extension occurs by coalescence of voids with the crack tip. This fracture mechanism and the assessment of crack in ductile material are better assessed with the help of fracture parameters. There are some fracture parameters which defines the fracture behaviour of ductile material, viz. stress intensity factor (K), energy release rate (G), crack tip opening displacement (CTOD), J-integral (J) and characteristic distance (lc). Stress intensity factor (K) is the magnitude of the ideal crack tip stress field for a particular mode in a homogenous linear-elastic body. Whereas, energy release rate (G) is the energy dissipated during fracture per unit of newly created fracture surface area. Similarly, crack tip opening displacement (CTOD) is the crack displacement due to elastic and plastic deformation at various defined locations near the original crack tip.

The J-integral define as a mathematical expression, a line or surface integral that encloses the crack front from one crack surface to the other and used to characterize the local stress-strain field around the crack front. It is used for highly ductile material such as nickel, iron, aluminum etc. Another fracture parameter is characteristic distance (Lc).

The characteristic distance (Lc) defined as the distance between the crack tip and the void responsible for eventual coalescence with the crack tip. Although approximate, (Lc) assumes a special significance since it links the fracture toughness to the microscopic mechanism considered responsible for ductile fracture. The knowledge of the "characteristic distance" is also crucial for designing the size of mesh in the finite element simulations of material crack growth using damage mechanics principles.

Conceptually, these fracture parameters should be an intrinsic material property that should not vary with changes in specimen size, crack length, thickness of material etc. The geometry dependency of some of these fracture parameters (like J) has been shown in the literature through experimental results. This been the reason ASTM code specified the fracture specimen dimensions criteria to be meet out for the geometry

independent evaluation of these fracture parameters experimentally. Fracture parameter (J) has also been shown, numerically, to be dependent on the thickness of fracture specimen. Experimental evaluation of characteristic distance has been shown experimentally in the literature and there is also some literature on the numerical assessment of characteristic distance using two-dimensional FEM analysis. Also, there is not much work (experimental as well as numerical) available in the literature related to the dependency of "characteristic distance" on the fracture specimen geometry.

The present research work is an attempt to understand numerically, the geometry dependency of "characteristic distance" using three-dimensional FEM analysis. The variation of "characteristic distance" parameter across the fracture specimen thickness will also be studied. The objective of the present study has been given in the following section.

- To establish "Characteristic distance" prediction methodology using three-dimensional FEM analysis.
- To study the variation of lc across the specimen thickness using 3D FEM analysis results.
- Validation of numerical model with experimental result
- To understand the effect of fracture specimen thickness on the "Characteristic distance".
- To understand the effect of change in temperature on the "Characteristic distance".
- Study has been done using Armco iron tested at different temperatures (303K, 383K, 423K, 473K, 573K)
- Finally, recommendations based on the present study.

The problem associated with component failure due to formation of voids of second phase particles or grain boundaries in the vicinity of the crack tip and the growth of voids. The importance of determining characteristic distance has special significance since it links the fracture toughness to the microscopic mechanism considered responsible for ductile fracture.

A. Stress-strain curves

Stress-strain curves are an extremely important graphical measure of a material's mechanical properties, and all students of Mechanics of Materials will encounter them often. However, they are not without some subtlety, especially in the case of ductile materials that can undergo substantial geometrical change during testing. This module will provide an introductory discussion of several points needed to interpret these curves and in doing so will also provide a preliminary overview of several aspects of a material's mechanical properties.

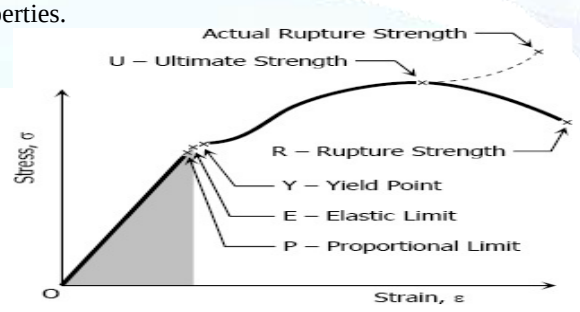

Fig. 1 Stress-strain curve

1. Proportional Limit (Hooke's Law)

From the origin O to the point called proportional limit, the stress-strain curve is a straight line. This linear relation between elongation and the axial force causing was first noticed by Sir Robert Hooke in 1678 and is called Hooke's Law that within the proportional limit, the stress is directly proportional to strain or

$$\sigma \propto \varepsilon$$

$$\sigma = E\varepsilon$$

Where σ is stress and ε is called strain, E is called Modulus of Elasticity or Young's Modulus.

2. Elastic Limit

The elastic limit is the limit beyond which the material will no longer go back to its original shape when the load is removed, or it is the maximum stress that may e developed such that there is no permanent or residual deformation when the load is entirely removed.

3. Elastic and Plastic Ranges

The region in stress-strain diagram from O to P is called the elastic range. The region from P to R is called the plastic range.

4. Yield Point

Yield point is the point at which the material will have an appreciable elongation or yielding without any increase in load.

5. Ultimate Strength

The maximum ordinate in the stress-strain diagram is the ultimate strength or tensile strength.

6. Rapture Strength

Rapture strength is the strength of the material at rupture. This is also known as the breaking strength.

7. Modulus of Resilience

Modulus of resilience is the work done on a unit volume of material as the force is gradually increased from O to P, in N•m/m3. This may be calculated as the area under the stress-strain curve from the origin O to up to the elastic limit E (the shaded area in the figure). The resilience of the material is its ability to absorb energy without creating a permanent distortion.

8. Modulus of Toughness

Modulus of toughness is the work done on a unit volume of material as the force is gradually increased from O to R, in $N•m/m^3$. This may be calculated as the area under the entire stress-strain curve (from O to R). The toughness of a material is its ability to absorb energy without causing it to break.

9. Working Stress, Allowable Stress, and Factor of Safety

Working stress is defined as the actual stress of a material under a given loading. The maximum safe stress that a material can carry is termed as the allowable stress. The allowable stress should be limited to values not exceeding the proportional limit. However, since proportional limit is difficult to determine accurately, the allowable tress is taken as either the yield point or ultimate strength divided by a factor of safety. The ratio of this strength (ultimate or yield strength) to allowable strength is called the factor of safety.

B. Fracture toughness based Characteristic Distance

The characteristic distance defined as the distance b/w the crack tip & the void responsible for eventual coalescence with the crack tip. Nucleation of these voids is generally associated with the presence of second phase particles or grain boundaries in the vicinity of the crack tip. Although approximate, assumes a special significance since it links the fracture toughness to the microscopic mechanism considered responsible for ductile fracture.

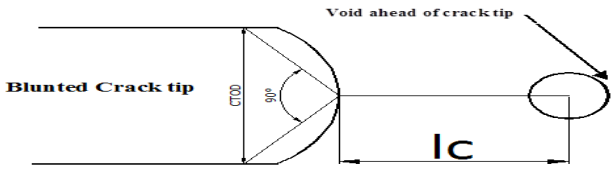

Fig. 2 Characteristic Distance (Pictorial View)

C. Types of fracture

1. Brittle fracture

The brittle fracture, no apparent plastic deformation takes place before fracture. In brittle crystalline materials, fracture can occur by cleavage as the result of tensile stress acting normal to crystallographic planes with low bonding (cleavage planes). In amorphous solids, by contrast, the lack of a crystalline structure results in a conchoidal fracture, with cracks proceeding normal to the applied tension.

2. Ductile fracture

In ductile fracture, extensive plastic deformation takes place before fracture. The terms rupture or ductile rupture describes the ultimate failure of tough ductile materials loaded in tension. Rather than cracking, the material "pulls apart," generally leaving a rough surface. In this case there is slow propagation and absorption of large amount energy before fracture. Many ductile metals, especially materials with high purity, can sustain very large deformation of 50–100% or more strain before fracture under favourable loading condition and environmental condition. The strain at which the fracture happens is controlled by the purity of the materials. At room temperature, pure iron can undergo deformation up to 100% strain before breaking, while cast iron or high-carbon steels can barely sustain 3% of strain. Because ductile rupture involves a high degree of plastic deformation, the fracture behaviours of a propagating crack as modelled above changes fundamentally. Some of the energy from stress concentrations at the crack tips is dissipated by plastic deformation before the crack actually propagates.

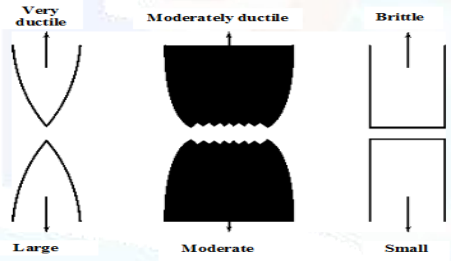

Fig. 3 Ductile Vs Brittle Failure

D. Mode of fracture failure

There are three ways of applying a force to enable a crack to propagate:

Mode I crack – Opening mode (a tensile stress normal to the plane of the crack)

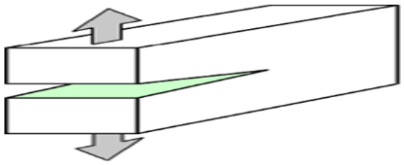

Fig. 4 Mode I (Tension, Opening)

Modes II crack – Sliding mode (a shear stress acting parallel to the plane of the crack and perpendicular to the crack front)

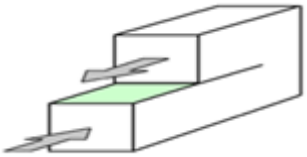

Fig. 5 Mode II (In-Plane Shear, Sliding)

Mode III crack – Tearing mode (a shear stress acting parallel to the plane of the crack and parallel to the crack front)

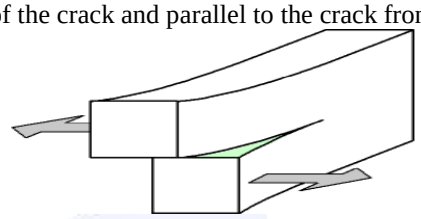

Fig. 6 Mode III (Out-Of-Plane Shear, Tearing)

E. Griffith's Analysis

The elliptical shape of the opening within a loaded body degenerates into a crack; the theoretical stresses at the end of the major axis tend to infinity. It becomes clear that while the stress concentration factor indicates the degree of the elevation of the local stress, the factor by itself is not a criterion of failure and it does not explain why a distinctly sharp crack does not produce a structural failure. Griffith was first to put forth a rational theory of fracture mechanics concerned with the specific conditions under which a small, sharp crack in a stressed body becomes unstable.

Since Griffith's approach to this problem was by way of energy, rather than the traditional force and stress, the entire idea was rather foreign at the time. Griffith regarded Inglis's stress concentration as a mechanism for converting strain energy into fracture energy. Such a mechanism, of course, can only work under a continuous supply of energy. If such a supply dries up, then the fracture process must stop.

Griffith assumed that incipient fracture in ideally brittle materials takes place when the elastic energy supplied at the crack tip is equal to or greater than the energy required to create new crack surfaces. His analysis was based on a model in the form of an elliptical cutout of length 2h, where for a very small dimension b (minor half-axis) and sharp corner radius, the cutout cussion the symbol h, standing for major half-axis of the ellipse, is changed to a, denoting crack length. Additional conditions required in analysing crack extension include. The stresses ahead of the crack tip must reach a critical magnitude. The total energy of the system must be reduced during crack extension. As stated previously in connection with stress trajectories, the state of stress in the y–x plane at the tip of the crack is expected to be at least biaxial. If the tip of the crack has a finite radius, it is also a free surface and the stress along the x-axis at x = a must be zero, while the stress along the y-axis at the same point attains a maximum value. The free faces of the plate carry no stresses.

The term plane stress, as used in the science of fracture mechanics, defines a state of stress in which one of the principal stresses is zero. This condition may be found in those applications where the thickness of a machine member or a structural element is small compared to other dimensions. The term plane strain, used in conjunction with the various definitions and criteria of fracture mechanics, refers to the state of a constraint in the vicinity of the crack tip. This situation

develops when the surrounding material prevents, say, contraction so that a high tension develops in the thickness direction. In essence we have a triaxial state of stress, and for a complete constraint, the strain in the z-direction (normal to the x–y plane in Fig.7) is zero.

The foregoing description of stress and strain conditions may be summarized in simple mathematical terms.

Plane stress:

$$\varepsilon_z = -\nu\frac{\sigma_x}{E} - \nu\frac{\sigma_y}{E}$$

Plane strain:

$$\varepsilon_z = \frac{\sigma_z}{E} - \nu\frac{\sigma_x}{E} - \nu\frac{\sigma_y}{E} = 0$$

from which

$$\sigma_z = \nu(\sigma_x + \sigma_y)$$

The stress given by Eq. cannot exist at the free surface although it can build up rather quickly going inward through the thickness of the material. Broek notes that in the absence of and presence of at the surface, a small dimple can develop. Since in practice a complete constraint is unlikely, a triaxial state of stress rather than a plane-strain condition should exist. However, the state of stress may not always be totally dictated by thickness.

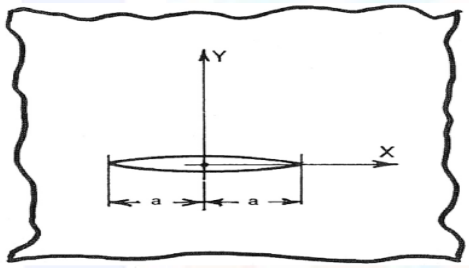

Fig. 7 Griffith crack form

F. Energy release rate, G

Griffith (1924) derived a criterion for crack growth using an energy approach. It is based on the concept that energy must be conserved in all processes. He proposed that when a crack grows the change (decrease) in the potential energy stored in the system, U, is balanced by the change (increase) in surface energy, S, due to the creation of new crack faces.

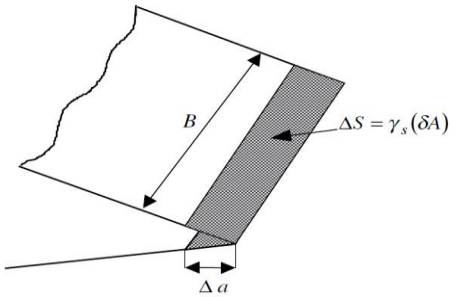

Fig. 8 Schematic of a crack growing by an amount Δa

Consider a through-thickness crack in a body of thickness B for fracture to occur energy must be conserved so,

$$\Delta U + \Delta S = 0$$

The change in surface energy, $\Delta S = \delta A\gamma_s$ where δA is the new surface area created and γ_s is the surface energy per unit area, as illustrated above. The change in area $\delta A = 2B\Delta\gamma_s$ (the factor of 2 arises because there are two crack faces).

Inserting these values and dividing across by BΔa we get

$$-\frac{1(\Delta U)}{B(\Delta a)} = 2\gamma_s$$

Rewriting as a partial derivative we get Griffith's relation,

$$-\frac{1(\delta U)}{B(\delta a)} = 2\gamma_s$$

If this equation is satisfied then crack growth will occur. The energy release rate, G is defined as

$$G = -\frac{1(\delta U)}{B(\delta a)}$$

In almost all situations $\frac{\delta U}{\delta a}$ is negative, i.e. when the crack grows the potential energy decreases, so G is positive. Note that the 1/B term is often left out and U is then the potential energy per unit thickness. G has units J/m^2, N/m and is the amount of energy released per unit crack growth per unit thickness. It is a measure of the energy provided by the system to grow the crack and depends on the material, the geometry and the loading of the system. The surface energy, γ_s, depends only on the material and environment, e.g. temperature, pressure etc., and not on loading or crack geometry.

From the above, a crack will extend when

$$G \geq 2\gamma_s = G_c$$

Where G is crack driving force and material toughness.

It was found that while Griffith's theory worked well for very brittle materials such as glass it could not be used for more ductile materials such as metals or polymers. The amount of energy required for crack was found to be much greater than 2 γ_s for most engineering materials. The result was therefore only of academic interest and not much attention was paid to this work outside the academic community.

In 1948 Irwin and Orowan independently proposed an extension to the Griffith theory, whereby the total energy required for crack growth is made up of surface energy and irreversible plastic work close to the crack tip:

$$\gamma = \gamma_s + \gamma_p$$

where γ_p is the plastic work dissipated in the material per unit crack surface area created.

$$-\frac{1(\delta U)}{B(\delta a)} \geq 2(\gamma_s + \gamma_p)$$

Or

$$G = -\frac{1(\delta U)}{B(\delta a)} \geq 2(\gamma_s + \gamma_p) = G_c$$

The Griffith and Irwin/Orowan approaches are mathematically equivalent; the only difference is in the interpretation of the material toughness Gc. In general Gc is obtained directly from fracture tests which will be discussed later and not from values of and The critical energy release rate, Gc, can be considered to be a material property like Young's Modulus or yield stress. It does not depend on the nature of loading of the crack or the crack shape, but will depend on things like temperature, environment etc.

G. Strain energy, energy release rate and compliance

The energy release rate G can be written in terms of the elastic (or elastic-plastic) compliance of a body. Before showing this, some general definitions will be given

1. Strain energy density

Strain energy density, W, is given by,

$$W = \int_0^{\varepsilon} \sigma d\varepsilon$$

Where σ is the stress tensor (matrix), ε is the strain tensor (matrix). Under uniaxial loading W is simply the area under the stress-strain curve (note: not the load displacement curve) as illustrated in Fig. 9 In general, the strain energy will not be constant throughout the body but will depend on position

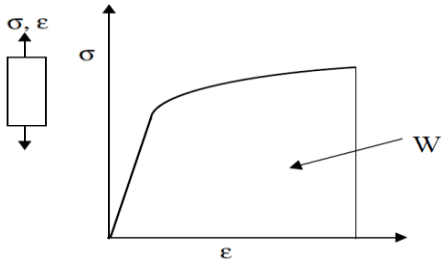

Fig. 9 Definition of strain energy density W under uniaxial loading

2. Elastic and plastic materials

For an elastic material all energy is recovered on unloading. For a plastic material, energy is dissipated. The strain energy density of an elastic material depends only on the current strain, while for a plastic material W depends on loading/unloading history. If the material is under continuous loading, W for an elastic and plastic material is the same. However, if there is total or partial unloading there is a difference. The response of elastic and an elastic-plastic material such as steel is shown in Fig. The elastic material unloads back along the loading path, i.e. no work is done in a cycle which in fact is the definition of an elastic material. For an elastic-plastic material there is generally an initial elastic regime where the stress-strain curve is linear (stress directly proportional to strain) and energy is recoverable and a nonlinear plastic regime where energy is dissipated (unrecoverable). Unloading is usually taken to follow the slope of the initial elastic region. There is then a permanent plastic deformation and the area under the curve gives the work done in a cycle.

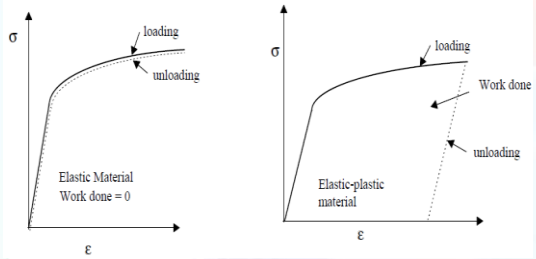

Fig. 10 Comparison between behaviour of an elastic material (left) and an elastic-plastic material (right)

An elastic material need not be a linear elastic material—there are elastic materials, e.g. rubbers, which are non-linear. However, the term elastic is often used as shorthand for linear elastic. For a linear elastic material,

$$\sigma = D\varepsilon$$

where D is the elasticity matrix and σ and ε are the stress and strain matrices.

$$W = \frac{1}{2}\sigma\varepsilon$$

In uniaxial loading

$$W = \sigma^2 / 2E$$

Power law hardening, a non-linear stress-strain law where strain is proportional to stress raised to a power, is often used to represent the plastic behaviour of materials

$$\sigma = D\varepsilon^{1/n}$$

where again D is a matrix of material constants and n is the strain hardening exponent, $1 \le n \le \infty$ In this case, it can be shown that,

$$W = \frac{n}{1+n}\sigma\varepsilon$$

H. Fracture mechanics

Fracture mechanics concerns the design and analysis of structures which contain cracks or flaws. On some size-scale all materials contain flaws either microscopic, due to cracked inclusions, debonded fibers etc., or macroscopic, due to corrosion, fatigue, welding flaws etc. Thus fracture mechanics is involved in any detailed design or safety assessment of a structure. As cracks can grow during service due to e.g. fatigue, fracture mechanics assessments are required throughout the life of a structure or component, not just at start of life. Clearly, the latter have a different mechanical behavior than the former and it is characterized according to the principles of fracture mechanics, which are divided into two areas. Linear Elastic Fracture Mechanics (LEFM) considers the fundamentals of linear elasticity theory, and Elastic Plastic Fracture Mechanics (EPFM) is for characterizing plastic behavior of ductile solids. (Nestor perez)

1. Linear Elastic Fracture Mechanics (LEFM)

It can be applied to plastically deforming materials provided the region of plastic deformation is small. This condition is called the small scale yielding condition. LEFM works well as long as the zone of non-linear effects (plasticity) is small compared to the crack size. However in many situations the influence of crack tip plasticity becomes important. There are two main issues:

- In order to obtain in a laboratory test, small specimens are preferred (for cost and convenience). However, to obtain a valid measurement for materials with high toughness or low yield strength a very large test specimen may be required.
- In real components there may be significant amounts of plasticity, so LEFM is no longer applicable. For these reasons we need to examine non-linear fracture mechanics where the inelastic near tip response is accounted for.

2. Elastic Plastic Fracture Mechanics (EPFM)

It is proposed to analyze the relatively large plastic zones. Elastic Plastic Fracture Mechanics (EPFM) assumes isotropic and elastic-plastic materials. Based on the assumption, the strain energy fields or opening displacement near the crack tips are calculated. When the energy or opening exceeds the critical value, the crack will grow.

Please note that although the term elastic-plastic is used in this approach, the material is merely nonlinear-elastic. In others words, the unloading curve of the so called elastic-plastic material in EPFM follows the original loading curve, instead of a parallel line to the linear loading part which is normally the case for true elastic-plastic materials.

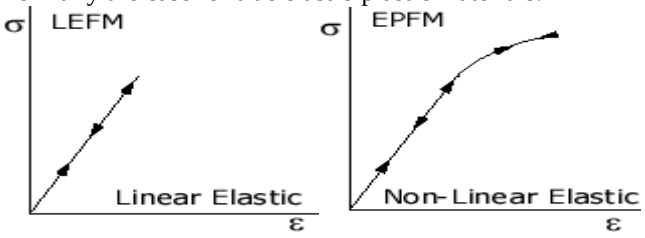

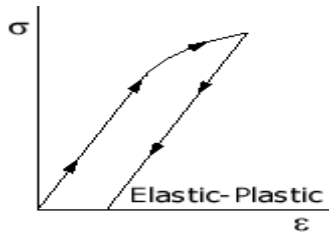

Fig. 11 Elastic plastic fracture mechanics

I. Concept of Stress Intensity

Many years after the Griffith fracture criterion for ideally brittle materials was established, Irwin and Orowan suggested a modification that would extend the Griffith theory to metals exhibiting plastic deformation. This modification was based on the idea that the resistance to crack extension was due to the combined effect of the elastic surface energy and the plastic-strain work Since the term $K = \gamma\sigma\sqrt{\Pi a}$, where K represents the intensity of the stress field at the tip of a through-thickness Griffith crack of length 2a, there must be a direct relationship between the stress intensity parameter K and the relevant material properties.

In this zone, the stress field is completely described by the stress intensity factor, K, and the stresses are given by the following equations:

$$\lim_{y\to 0} \sigma_{ij} = \frac{K_I}{\sqrt{2\Pi r}} f_{ij}^{I}(\theta)$$

$$\lim_{y\to 0} \sigma_{ij} = \frac{K_{II}}{\sqrt{2\Pi r}} f_{ij}^{II}(\theta)$$

$$\lim_{y\to 0} \sigma_{ij} = \frac{K_{III}}{\sqrt{2\Pi r}} f_{ij}^{III}(\theta)$$

The subscripts of K are usually given in roman numerals, K_I , K_{II} and K_{III} , which refer to the modes of loading. Hence KI describes the opening (tensile) mode where the displacement of the crack surface is perpendicular to the crack plane. The K_{II} parameter is applicable to the sliding, or in-plane, shearing mode, here the crack surface moves in the plane of the crack and, at the same time is normal to the leading edge of the crack. Finally, K_{III} refers to the tearing mode of external loading caused by out-of-plane shear. For practical reasons, Mode I is the most important, and therefore only the K_I parameter is considered vertical plane.

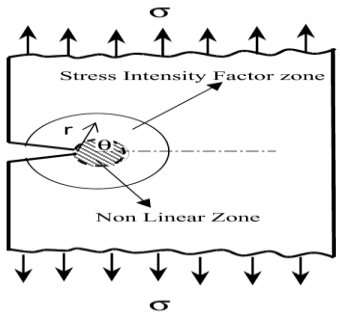

Fig. 12 Stress intensity zone (SI)

J. Crack Tip Opening Displacement (CTOD)

There are two common definitions of the crack tip opening displacement (CTOD): The opening displacement of the original crack tip. The displacement at the intersection of a 90° vertex with the crack flanks.

Fig. 13 CTOD of original crack tip

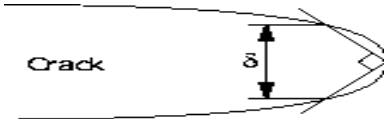

Fig. 14 CTOD of crack tip at intersection of 90 vertex

II. Literature Review

Long before 1921, when Griffith published his monumental theory on the rupture of solids, a number of pioneering results had appeared which gave evidence of the existence of a size effect on the strength of solids. These findings, which could be considered as a prelude to the Griffith theory, will now be briefly described. Leonardo da Vinci (1452-1519) ran tests to determine the strength of iron wires .He found an inverse relationship between the strength and the length, for wires of constant diameter.

Observe what the weight was that broke the wire, and in what part the wire broke... Then shorten this wire, at first by half, and see how much more weight it supports; and then make it one quarter of its original length, and so on, making various lengths and noting the weight that breaks each one and the place in which it breaks. Todhunter and Pearson refer to two experimental results nalogous to those of da Vinci. According to Lloyd (about 1830) found that the average strength of short iron bars is higher than that of long iron bars and Le Blanc (1839) established long iron wires to be weaker than short wires of the same diameter. Stanto and Batson reported the results of tests conducted on notched-bar specimens at the National Physical Laboratory, Teddington, after the First World War. From a series of tests it was obtained that the work of fracture per unit volume was ecreased as the specimen dimensions were increased. Analogous results were obtained by Docherty who found that the increase of the plastic work at fracture with the specimen size was smaller than that obtained from geometrical similarity of the strain patterns. This means that the specimens behaved in a more brittle fracture as their size was increased.

All these early results gave indication of the so-called size effect of the strength of solids, which is expressed by an increase in strength as the dimensions of the test piece decrease. Results at the U.S. Naval Research Laboratory on the strength of glass fibers corroborated the early findings of Leonardo da Vinci.

Fracture mechanics concerns the design and analysis of structures which contain cracks or flaws. On some size-scale all materials contain flaws either microscopic, due to cracked inclusions, debonded fibres etc., or macroscopic, due to corrosion, fatigue, welding flaws etc. Thus fracture mechanics is involved in any detailed design or safety assessment of a structure. As cracks can grow during service due to e.g. fatigue, fracture mechanics assessments are required throughout the life of a structure or component, not just at start of life. Fracture mechanics answers the questions: What is the largest sized crack that a structure can contain or the largest load the structure can bear for failure to be avoided. Studies in the US in the 1970s by the US National Bureau of Standards estimated

that "cost of fracture" due to accidents, overdesign of structures, inspection costs, repair and replacement was on the order of 120 billion dollars a year. While fracture cannot of course be avoided, they estimated that, if best fracture control technology at the time was applied, 35 billion dollars could be saved annually.

This indicates the importance of fracture mechanics to modern industrialised society. The topics of linear elastic fracture mechanics, elastic-plastic fracture mechanics and high temperature fracture mechanics (creep crack growth) are dealt with in this course. The energy release rate method of characterizing fracture is introduced and the K and HRR fields which characterise the crack tip fields under elastic and plastic/creep fracture respectively are derived. The principal mechanisms of fracture which control failure in the different regimes are also discussed. In the later part of the course, the application of these fracture mechanics principles in the assessment of the safety of components or structures with flaws through the use of standardized procedures is discussed. The approach taken in this course is somewhat different from that in Fundamentals of Fracture Mechanics (FFM) as here more emphasis is put on the mechanics involved and outlines of mathematical proofs of some of the fundamental fracture mechanics relationships are provided. There is some revision of the topics covered in FFM, particularly in the area of linear elastic fracture mechanics though the approach is a little different.

S. Nakamura et al. (1995) pointed out that the distributions of stress and strain in composite and cellular materials could differ significantly from the predictions of classical elasticity. For example, concentration of stress and strain around holes and cracks is consistently less than classical predictions. Generalized continuum theories such as micro polar (Cosserat) elasticity offer improved predictive power. In this article Saint-Venant end effects for self-equilibrated external forces in micro polar solids are investigated in two dimensions. A two dimensional finite element analyses is used which takes into account the extra degrees of freedom, to treat the problem of localized end loads acting upon a strip. The rate of decay of strain energy becomes slower in a two-dimensional strip as the micro polar characteristic length is increased (for sufficiently less than the strip width).

Ye Zhiming (1996) presented a comprehensive derivation of fracture process zone size which closely parallels similar work in fracture of metals and anisotropic solids, but is adapted to concrete. Some nonlinear mechanics models of concrete materials were discussed by using uniaxial stress assumptions. For uniaxial stress assumption, energy model and fracture model will be presented for nonlinear softening models. Finally, we make a comparison with those models.

J. Du, et al. (1998) investigated the effects of process zone on toughness and on R-curve behavior for a model, rubber-modified epoxy polymer. The system studied was one in which the bridging mechanism of toughening does not operate. The characteristic features of R-curve behavior, a rise in toughness with crack extension until an approximate steady state is reached, were observed using double-cantilever-beam tests. The evolution of the process zone was studied using transmission-optical microscopy. As the crack grew, the process zone appeared to fan out until it reached a steady-state thickness; it then remained a uniform size upon further crack advance. The features of the experimental R-curves were shown to be directly correlated to the evolution of the process zone. Furthermore, the effect of the portion of the process zone in the crack wake was examined by a series of experiments in which the wake was partially removed, and the R-curve re-established by subsequent loading. These experiments demonstrated that removal of the crack wake caused the crack-growth resistance to drop. The toughness then built back up to the steady-state value as the crack wake re-developed. This unambiguously demonstrated a contribution to toughening from the crack wake despite the absence of any observable bridging mechanism. These results support the accepted notion that an extrinsic toughening mechanism is responsible for the increased toughness observed upon adding rubber particles to an epoxy matrix.

J. Zhao et al. (2000) made parametric studies on the growing crack tip fields under quasi-static tensile loading with damage coupled power-law elastic-plastic constitutive equations. A two-sector demarcation scheme is used. The asymptotic orders and angular distributions of the stress and damage fields are obtained. The shapes of the process zone are also determined. The law of crack growth is formulated as well.

G.Z.Wang et al. (2002) studied characteristic distance, minimum fracture toughness and its temperature dependence for cleavage fracture in a C-Mn steel by the detailed finite element analysis combined with experimental observation and measurement. Results show that there is a minimum active zone for cleavage initiation and the minimum fracture toughness of steel results from the minimum active zone necessary. Corresponding to the minimum fracture toughness, the cleavage fracture ahead of a crack tip can only initiate in a distance range from the minimum distance determined by the lower boundary of the active zone to the maximum distance determined by its upper boundary. The reason for the occurrence of the minimum active zone and the factors influencing it are analyzed. The temperature dependence of the characteristic distance and minimum fracture toughness and its mechanism are also discussed.

Michael P.Wnuk et al. (2002) proposed a new law to describe the distribution of the cohesive forces present within the internally structured nonlinear zone that precedes the leading edge of a moving crack contained within a nonelastic solid. The nonlinear effects are modeled by the narrow strips emanating from the crack front and endowed with a certain internal structure (unlike the classic models of Barenblatt and Dugdale). The bulk of the material, though, is assumed to behave as linear elastic solid. Mathematical form the law resembles somewhat the Planck's formula used to explain radiation given off by a perfectly black body at very short wavelength of the visible light spectrum. With Sneddon's integral transformations employed and properly modified, the quantities essential in the Nonlinear Mechanics of Fracture have been quantified. In particular another so-called 'ubiquitous eta factor' is discussed and related to the material microstructure by means of a certain transcendental equation. The eta factor enters the formula for the specific work of fracture measured with specimens of various geometrical and loading configurations, and so far is known only empirically. Both the stationary and quasi-static crack problems are discussed. It has been shown that the variations in the microstructural parameters strongly affect the process zone along with the associated work of separation. The other important factors that influence the cohesive stress distribution and all the resulting fracture parameters, specifically those that are responsible for a ductile-to-brittle transition of fracture

mode, are the characteristics of the state of stress induced in the vicinity of the crack front. These 3D effects are best represented by the triaxiality parameter, defined as the ratio of the mean stress to the von Mises effective stress.

Yu.G. Matvienko (2004) presented a crack tip model with the cohesive zone ahead of a finite crack tip. The estimation of the length of the cohesive zone and the crack tip opening displacement is based on the comparison of the local stress concentration, according to Westergaard's theory, with the cohesive stress. To calculate the cohesive stress, von Mises yield condition at the boundary of the cohesive zone is employed for plane strain and plane stress. The model of the stress distribution with the maximum stress within the cohesive zone is discussed. Local criterion of brittle fracture and modelling of the fracture process zone by cohesive zone were used to describe fracture initiation at the hydride platelet in the process zone ahead of the crack tip. It was shown that the theoretical KIH - estimation applied to the case of mixed plane condition within the process zone is qualitatively consistent with experimental data for unirradiated Zr-2.5Nb alloy. In the framework of the proposed model, the theoretical value of KH IC for a single hydride platelet at the crack tip has been also estimated.

L.R. Botvina (2004) studied a common kinetic feature of multiple fractures of metallic specimens tested at different loading conditions and it is used for an analysis of seismic activity accompanying multiple formations of faults in the earth crust. The study revealed the similarity of basic regularities in the dynamics of seismicity before earthquake and in kinetics of damage accumulation before specimen fracture, estimated by acoustic emission and metallographic methods. The results obtained confirm the ideas of self-similarity and the hierarchical sequence of Multiple fractures and they provide a physical basis for prediction of the critical events at various scale levels.

K. Haidar et al. (2005) examined the correlation between the width of the fracture process zone, the parameters entering in the description of size effect (related to the dimension of the specimen especially), and the internal length in non-local constitutive relations for a model mortar material with a controlled macro-porosity. Experimental investigations on this material in compression, bending, acoustic emission measurements and their analysis are detailed. The experiments show a good agreement between the evolution of Bezant's size effect parameter and the evolution of the width of the FPZ. The internal length obtained with the help of inverse finite element analysis is also proportional to these quantities. This correlation provides a reasonable approximation of the internal length, from an experimental test on specimens of a single size directly, equipped with acoustic emission localization devices.

Wu Yan-qing et al. (2006) used cohesive zone model to simulate two-dimensional plane strain crack propagation at the grain level model including grain boundary zones. Simulated results show that the original crack-tip may not be separated firstly in an elastic-viscoplastic polycrystals. The grain interior's material properties (e.g. strain rate sensitivity) characterize the competitions between plastic and cohesive energy dissipation mechanisms. The higher the strain rate sensitivity is, the larger amount of the external work is transformed into plastic dissipation energy than into cohesive energy, which delays the cohesive zone rupturing. With the strain rate sensitivity decreased, the material property tends to approach the elastic-plastic responses. In this case, the plastic dissipation energy decreases and the cohesive dissipation energy increases which accelerates the cohesive zones debonding. Increasing the cohesive strength or the critical separation displacement will reduce the stress triaxiality at grain interiors and grain boundaries. Enhancing the cohesive zones ductility can improve the matrix materials resistance to void damage.

H. Hadjab.S et al. (2007) used Scanning Electron Microscope (SEM) to understand the micro level aspect of the Fracture Process Zone (FPZ) in a concrete beam. It is mainly based on the preparation and analyzing samples which are considered as being a very important part of SEM (poor preparation techniques can lead to erroneous diagnosis of the concrete study). Numerically, the fractureof concrete requires the consideration of progressive damage, which is usually modeled by a constitutive law. This latest relies on numerical methods to obtain adequate solutions. It is shown herein that by using the Object Oriented Finite Element Method (OOFEM), obtained results agreed more or less with those of others researchers. On the other side, experimental results compromise thoseobtained by the use of the non-local isotropic damage model. It is finally proven throughout this study that the FPZ is defined by two parameters: the length and the width.

Xiaozhi Hu et al. (2007) studied the size effect on strength of cementitious materials successfully many years ago by a crack-bridging model through detailing the influence of the resistance R-curve behaviour on quasi-brittle fracture. The condition that specimens of different sizes have to be geometrically similar, commonly assumed for size effect study, was proven unnecessary. The present study emphasizing the interaction between the fracture process zone and structure boundary agrees with the crack-bridging analysis, and further points out that physical size itself is not the key mechanism for the apparent size effect.

Jacob L. Jones et al. (2007) proposed that non-180_ domain switching leads to fracture toughness enhancement in ferro elastic materials. Using a high-energy synchrotron X-ray source and a two-dimensional detector in transmission geometry, non-180_ domain switching and crystallographic lattice strains were measured in situ around a crack tip in a soft tetragonal lead zirconate titanate ceramic. At and below the initiation toughness, the process zone size, spatial distribution of preferred domain orientations, and lattice strains near the crack tip are a strong function of direction within the plane of the compact tension specimen. Deviatoric stresses and strains calculated using a finite element model and projected to the same directions measured in diffraction correlate with the measured spatial distributions and directional dependencies. Some preferred orientations remain in the crack wake after the crack has propagated; within the crack wake, the tetragonal 001 axis has a preferred orientation both perpendiculars to the crack face and toward the crack front.

Sanjeev Saxena et al. (2007) studied several methods to understand the process of crack initiation and propagation in ductile materials. In an attempt to achieve an overall understanding, some of these techniques were studied using a large deformation based finite element method (FEM). In the current investigation, typical crack tip blunting prior to ductile fracture behavior of a standard (CT) specimen under mode I loading condition was simulated using FEM. An attempt was made to understand the ductile fracture by numerically determining the ductile fracture toughness at three length scales: macroscopic scale (load–displacement method), mesoscopic

scale (path-integral method) and microscopic scale (stretch zone width method). In addition, the characteristic distance (lc), commonly defined as the distance between the crack tip and the void responsible for eventual coalescence with the crack tip, was also studied. Although approximate, lc assumes a special significance since it links the fracture toughness to the microscopic mechanism considered responsible for ductile fracture.

E. E. Kurchakov et al. (2008) studied the plastic zone at a crack in an anisotropic body in the case of a generalized plane stress state. Strains are assumed small. The body is rectangular and thin and has a mode I crack at the center. The governing equations are written for the components of the displacement vector. By numerically solving the boundary-value problem, we can describe how the plastic zone forms and, in particular, can establish the effect of the crack length on the size and shape of the plastic zone.

A. V. Kashtanov et al. (2008) proposed a new approach describing the dynamic fracture as a process of nucleation and subsequent propagation of a nonlinear wave of microfracture. The equation describing the microfracture evolution is derived from the transfer equation and a stochastic diffusion-type description of damage redistribution. The physical meaning of the corresponding parameters is clarified by the mass conservation and the incubation time criterion of fracture. Finally the process of dynamic macrocrack nucleation is simulated.

Sanjeev Saxena et al. (2009) addressed numerical determination of stretch zone width and its critical value. The proposed method is based on the highly deformed stretch zone that is defined as stretch zone width, expected to be better than the half of the crack tip opening distance which in turn determined using 45 line methods. The investigation essentially comprises a number of finite element analyses of compact tension test, using tensile test data. The proposed methodology also provides insight into the mechanism involved in the creation of stretch zone.

Franck Vernerey et al. (2009) proposed a multiscale process zone model based on linear elastic fracture mechanics and a multiscale micromorphic theory. By computing the stress intensity factor in a K-dominant region while maintaining the mechanism of failure in the process zone, this model allows the evaluation of the fracture toughness of hierarchical materials as a function of their microstructural properties. After introducing a multi-length scale finite element formulation, an application is presented for high strength alloys, whose microstructure typically contains two populations of particles at different length scales. For this material, the design parameters comprise of the strength of the matrix–particle interface, the particle volume fraction and the strain-hardening of the matrix. Using the proposed framework, trends in the fracture toughness are computed as a function of design parameters, showing potential applications in computational materials design.

K.Y. Volokh (2010) proposed that the characteristic length ~0.2 mm of natural rubber, which presents the width of a narrow zone where damage localizes initiating a crack. It is remarkable that our direct calculation is based on the results of the macroscopic experiments only.

A. M. Linkov (2010) stressed upon the role of a structural parameter having the dimension of length, and also the importance of the Novozhilov–Neuber force criterion; this criterion allows obtaining simple and far-reaching generalizations. The main attention is paid to the results obtained by the author either in collaboration with Professor Novozhilov or as a result of close communication with him for almost two decades. The force treatment of the strict stability condition, which implies using a linear softening in the crack tip region, and the estimate of the maximal speed of crack propagation, based on a structural-time criterion, are performed for the first time.

A. Kaminsky et al. (2010) analyzed the influence of longitudinal loading on the size and shape of the plastic zone near a crack in an anisotropic body. A generalized plane stress state is considered. A relevant boundary-value problem is solved numerically to study the behavior of the main plastic zone at the crack tip, a new plastic zone above the crack, and an additional plastic zone on the lateral surface, which merge to form a single plastic zone.

B. Yang et al. (2010) proposed a cohesive zone model to model crack growth with a part-through process zone in a thin solid. With the solid being modeled in Kirchhoff's plate theory, the crack with a relatively long, inclined front is modeled as a line discontinuity with a finite cohesive zone within the plate. A cohesive force law is adopted to capture the effect of residual strength and residual rigidity of a plate cross-section gradually cracking through the thickness. It is derived by a plane-strain elasticity analysis of a cross section normal to the part-through crack. It is then applied in the plate formulation of a line crack to simulate its propagation within the plate plane. This model essentially resolves the originally three- dimensional crack problem in two hierarchical steps, i.e., in the thickness and in the in-plane directions. In the present study, the bending case is considered. A boundary element method is applied to numerically derive the cohesive force law and simulate the crack growth in a thin titanium- alloy plate. The computational efficiency of the model is demonstrated. The plate is shown to fracture in a nominally brittle or ductile manner depending on its thickness.

E. Sarris et al. (2010) studied the importance of the cohesive zone in the modeling of a fluid driven fracture under plain strain conditions. The fracture is driven by pumping of an incompressible viscous fluid at the fracture inlet. Rock deformation is modeled for linear elastic and poroelastic solids. Fluid flow in the fracture is modeled by lubrication theory. The cohesive zone approach is used as the fracture propagation criterion. Finite element analysis was used to compute the solution for the crack length, the fracture opening and propagation pressure as a function of the time and distance from the wellbore. It is demonstrated that the crack profiles and the propagation pressures are larger in the case of elastic-softening cohesive model compared to the results of the rigid-softening cohesive model for both elastic and poroelastic cohesive solids. It is found that the results are affected by the slope of the loading branch of the cohesive model and they are nearly unaffected from the exact form of the softening branch. Furthermore, the size of the process zone, the fracture geometry and the propagation pressure increase with increasing confining stresses. These results may explain partially the discrepancies in net-pressures between field measurements and conventional model predictions.

Sanjeev Saxena et al. (2010) presented large deformation FEM analyses in SA333Gr.6 carbon steel material, to demonstrate the assessment of SZWc value that leads to JSZWc and finally compares with the respective experimental results. It also includes numerical prediction of specimen J–R curve using Gurson–Tvergaard–Needleman parameters obtain

from tensile specimen tests. Using numerically predicted results, the crack initiation and instability stages in circumferentially through-wall cracked elbows is finally predicted and compares with experimental results. The present study gives evidence that the non-linear FEM analysis supported with proper tensile test data can be helpful in assessing the safety of bend pipes with through-wall crack.

III. Problem Formulation (Experimental Tested Data Used)

A. Stress-strain curves

Chemical composition of the material is taken from literature in which test had been conducted on Armco iron. The chemical composition of the material is shown in table I (M.Srinivas, 1991)

TABLE I
CHEMICAL COMPOSITION (IN WT. %) OF ARMCO IRON

Elements	*Wt%*
C	***0.008***
Mn	***0.03***
P	***0.006***
S	***0.005***
Fe	***Bal.***
Cr	***-***
Ni	***-***

B. Tensile tested data

Using Armco iron material, tensile tests were conducted at temperatures ranging from 298K to 573 K. Cylindrical tensile specimens of 15 mm gauge length and 4.5 mm gauge diameter had been used and tested at a nominal strain rate of 10^{-3} s^{-1}. The results of tensile test of the material tested at different temperatures have been given in Table II.

TABLE III
TENSILE TEST RESULTS

Temperature	*E(Gpa)*	*n*	σ_y *(MPa)*	σ_u *(MPa)*
RT (298°K)	***196***	***0.29***	***189***	***296***
383°K	***191***	***0.30***	***151***	***338***
423°K	***187***	***0.41***	***150***	***385***
473°K	***180***	***0.48***	***148***	***404***
573°K	***175***	***0.38***	***146***	***404***

C. Fracture specimen tested data

The ductile fracture toughness J_{ic} was evaluated at temperatures 298K-573 K employing the multiple specimens J-R curve technique as reported in the literature. The ramp rate during loading was kept constant at 8.33×10-6 m/s(0.5 mm/min).Compact tension specimens of 25 mm thickness were used at all the test temperatures excepting at the ambient temperature at which 50 mm thick specimens were utilized. The temperatures between 343K and 573 K were achieved by enclosing the specimens in an Instron environmental chamber. The characteristic distance is reportedly been obtained at room temperature using the SEM micrographs of the sectioned surfaces of interrupted test samples of Armco iron of grain size 78 μm. The experimental results of fracture test are given in Table III.

TABLE IIIII
FRACTURE TEST RESULTS

Temperature	*n*	J_{SZW} *(N/mm)*	*Lc (mm)*
RT (298°K)	***0.29***	***165***	***110***
383°K	***0.30***	***230***	***----***
423°K	***0.41***	***260***	***----***
473°K	***0.48***	***290***	***----***
573°K	***0.38***	***280***	***----***

IV. Prediction of Characteristic Distance Using FEM

The knowledge of the characteristic length is crucial for the finite element simulations of material failure because it allows regularizing the problem by suppressing the so-called pathological mesh sensitivity on the crack growth simulations. The latter means that the characteristic length sets the size of the finite elements that should be used in the areas where failure propagates. The present investigation three-dimensional FEM analyses have been carried out using ABAQUS FEM software. The numerical results are then evaluated for the numerical assessment of characteristic distance. The numerical predicted Lc value is then validated with experimental results at room temperature. The present numerical study have been carried our on Armco iron material tested at various temperature. The numerical studies have been carried out using the compact tension specimen of different thickness, as given in Table IV.

TABLE IVV
DIFFERENT THICKNESS OF CT SPECIMEN CONSIDERED IN THE STUDY

Sl. No.	*Thickness (mm)*	*Parameter*	*FEM*
1	***100 mm thick***	***Characteristic Distance***	***YES***
2	***50 mm thick***	***Characteristic Distance***	***YES***
3	***25 mm thick***	***Characteristic Distance***	***YES***
4	***12.5 mm thick***	***Characteristic Distance***	***YES***
5	***6.25 mm thick***	***Characteristic Distance***	***YES***
6	***3.125 mm thick***	***Characteristic Distance***	***YES***

A. Numerical prediction methodology

Characteristic distance is numerically predicted using methodology proposed by Saxena et al. (2007) which is energy based using material's tensile test data (true stress strain curve). Following this the critical energy density used to delineate the highly stretched region is defined on the material's true stress–strain curve as the energy density integral at the critical strain (εc) corresponding to onset of necking in tensile specimen or strain hardening exponent (n) for the specific case of power law variation of material's true stress–strain curve, given as:

$$E_{Crit.} = \int_0^n \sigma d\varepsilon$$

Where n is strain-hardening coefficient in power law corresponding to onset of necking.

The fracture energy density at which critical characteristic distance is predicted is given by:

$$E_{Fract.} = \int_0^{\varepsilon_f} \sigma d\varepsilon$$

Where εf is the fracture strain of the ductile material.

Using the above equation the energy density obtained is given in Table V.

TABLE V

CRITICAL AND FRACTURE ENERGY DENSITIES USED

Temperature	*n*	*Critical Energy Density (MJ/m^3)*	*Fracture Energy Density (MJ/ m^3)*
RT (298°K)	***0.29***	***92***	***1357***
383°K	***0.30***	***105***	***1396***
423°K	***0.41***	***148***	***1480***
473°K	***0.48***	***183***	***1565***
573°K	***0.38***	***154***	***1735***

B. Numerical FEM model

To validate the numerical methodology using three dimensions FEM analysis; the experimental results of Armco iron tested at room temperature were used. The numerical prediction work is further extended to higher temperatures to see the temperature variation on the characteristic distance value. To further study the effect of thickness, different thickness numerical FEM models of CT specimen have been done. The investigation was limited to CT specimen analysis subjected to mode-I type of loading. To have better understanding of the variation of fracture parameters across the thickness, one-fourth 3D FEM model of CT specimen have been used. The typical mesh used in the FEM model is given in Fig. 15.

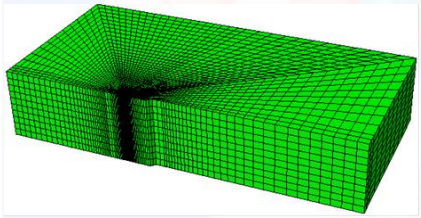

ELEMENT SIZE VARIATION

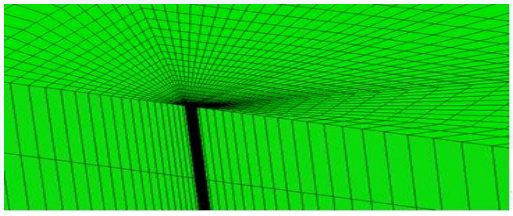

MESH NEAR THE CRACK FRONT

Fig. 15 Typical FEM model of CT specimen

The symmetry in this case permits consideration of only one fourth of the specimen geometry for computational economy. The analyses were done using commercial FEM software ABAQUS. The mesh was constructed with eight noded brick elements as used by Saxena et al, 2007. The mesh convergence study was done in the thickness direction to decide the number of elements in FEM model to be used in thickness direction.

C. Mesh convergence study

The convergence of FEM mesh used in two-dimensional model is already checked in the literature. Same size of elements is used in two directions. To decide the number of elements in the thickness direction, in the FEM model the number of elements in the thickness direction were varied from three, five, ten, fifteen and, twenty elements. Fig. 16 showed the variation of characteristic distance due to the change in the number of elements in the thickness direction.

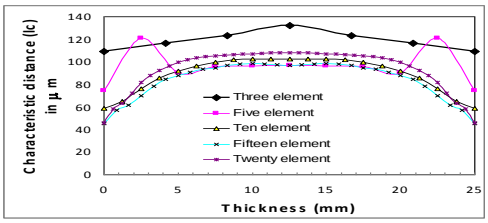

Fig. 16 Characteristic distance variation with number of elements in thickness direction

The average value of 'characteristic distance' near the mid thickness of specimen is taken as reference for the comparison of variation in magnitude of numerically predicted 'characteristic distance' value due to the change of number of elements in the thickness direction. Fig. 17 showed the variation of 'characteristic distance' value with the increase in number of elements in thickness direction. Initially when the there are three elements in the thickness direction, the percentage variation of Lc value is 29%. With the increase in number of elements in the thickness direction the Lc value started converging, which can be seen with the average percentage change of 5% after ten numbers of elements in the thickness direction. Therefore, in all the FEM model ten elements have been used though out the numerical study.

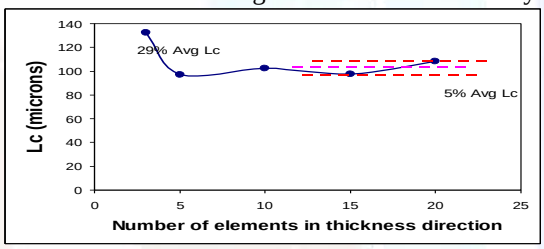

Fig. 17 Variation of average Lc with number of elements in thickness direction

D. Numerical prediction of characteristic distance

The FEM analysis was carried out up-to the stage where maximum energy density exceeds the fracture energy density of the material at a particular temperature. At this stage characteristic is obtained using the critical energy density of the material. Fig. 18 showed the demarcation of characteristic distance at a plane in 3D FEM model.

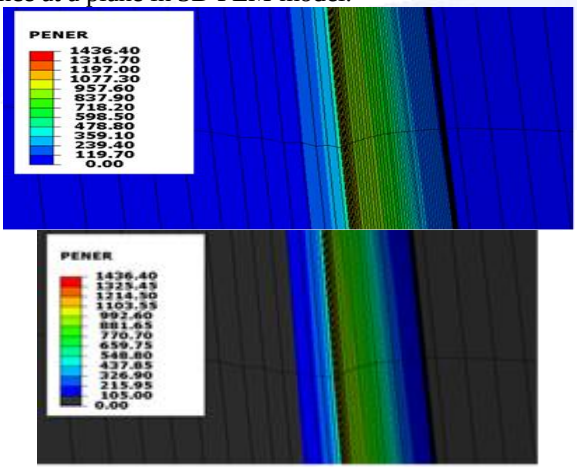

Fig. 18 Demarcation of characteristic distance at a plane

E. Validation of numerical model with experimental results

The numerical predicted result of characteristic distance results is required to be compared with experimentally determined results, as available in the literature to validate the numerical model used in the present study. Experimentally tested Characteristic distance value (110μm) of Armco iron material obtained at room temperature using 50mm thickness CT specimen are available in the literature. Therefore, to validate the numerical model, 50mm thick CT specimen is used and the variation of Characteristic distance is plotted using room temperature material property. Fig. 19 showed the variation of characteristic distance across the fracture specimen thickness.

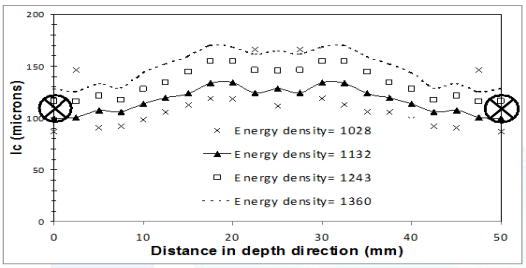

Fig. 19 Validation of numerical results with experimental result

From the figure it can be seen that the experimental obtained characteristic distance value compares reasonably well with the numerically predicted characteristic distance value, thus validates the present numerical model.

F. Variation of 'characteristic distance' with thickness and temperature

After validating the numerical model, the numerical prediction results are further extended to understand the variation of 'characteristic distance' due to the change in fracture specimen thickness and temperature. In three-dimensional FEM model, different thicknesses of CT specimen considered in the present study are 3.125mm, 6.25mm, 12.5mm, 25mm, 50mm and 100mm thick. To understand the variation of characteristic distance due to the change in temperature, five different test temperature tensile results are considered in the present study. The tensile properties of different temperature that are considered in the present study are room temperature (298°K), 383°K, 423°K, 473°K and 573°K. The Fig. 20 to Fig. 25 showed FEM model, von Mises stress distribution, variation of plastic energy density and the demarcation of characteristic distance using different thickness of compact tension specimen. The figures showed results at a temperature of 423°K. The predicted results of characteristic distance using different thickness of fracture specimen and using different temperature results are compared to understand the trends of characteristic distance variation due to these changes. The fracture specimen thickness requirement given in ASTM 1820, to obtain valid (geometry independent) fracture parameter, is also checked, in terms of 'characteristic distance'.

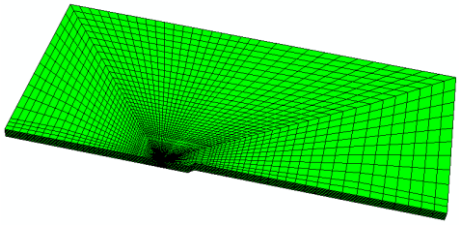

(a) FEM mesh

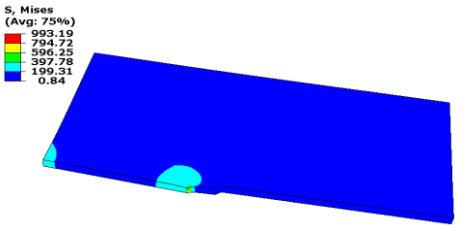

(b) vonMisses Stress

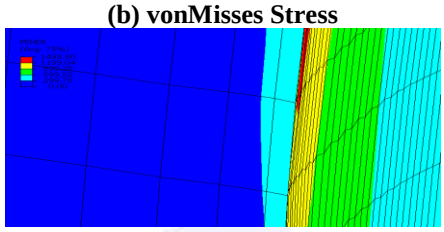

(c) Variation of energy

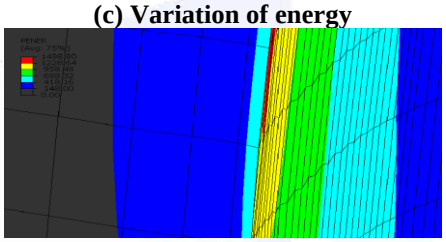

(d) Demarcation of Lc

Fig. 20 Compact tension Specimen (3.125mm thick, 423°K temperature)

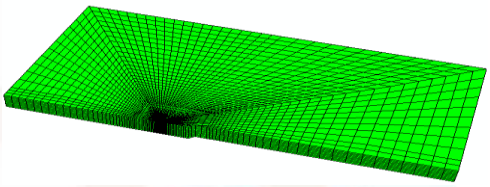

(a) FEM mesh

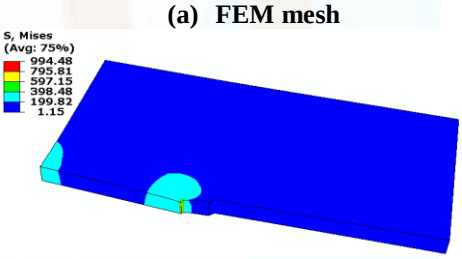

(b) vonMisses Stress

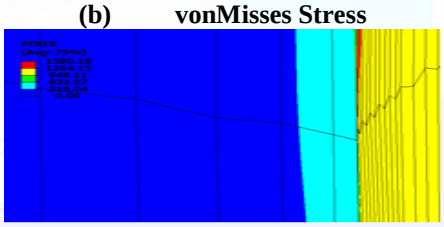

(c) Variation of energy

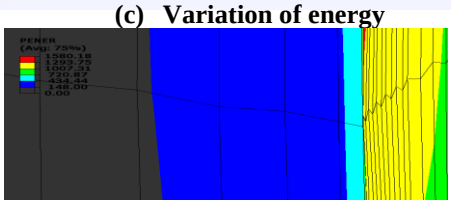

(d) **Demarcation of Lc**

Fig. 21 Compact tension Specimen (6.25mm thick, 423oK temperature)

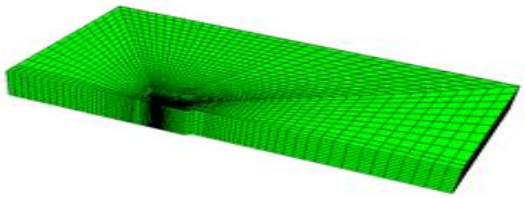

(a) FEM mesh

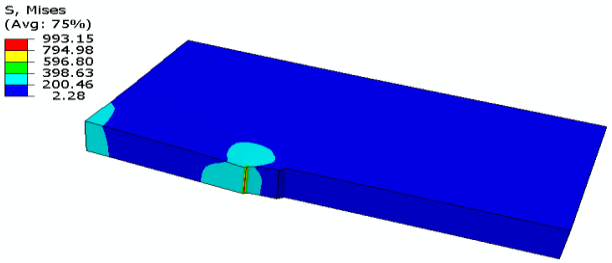

(b) vonMises Stress

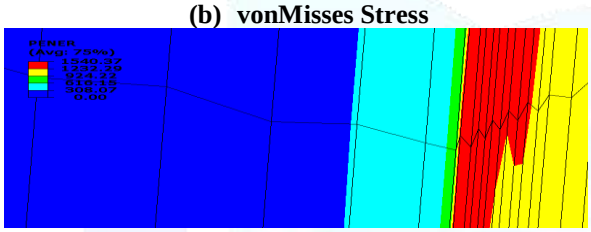

(c) Variation of energy

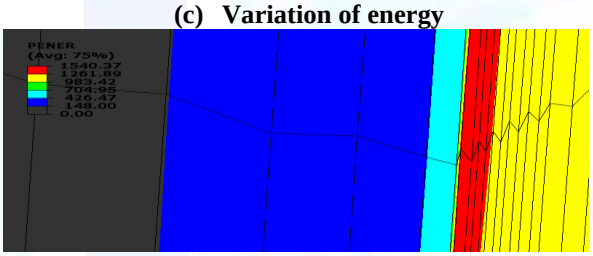

(d) Demarcation of Lc

Fig. 22 Compact tension Specimen (12.5mm thick, 423oK temperature)

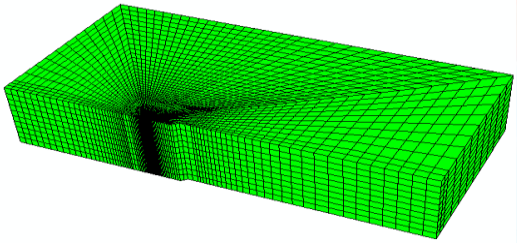

(a) FEM mesh

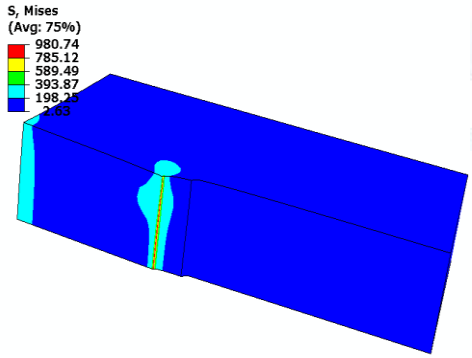

(b) vonMises Stress

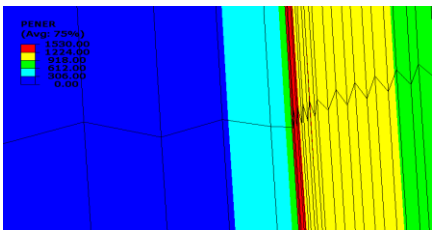

(c) Variation of energy

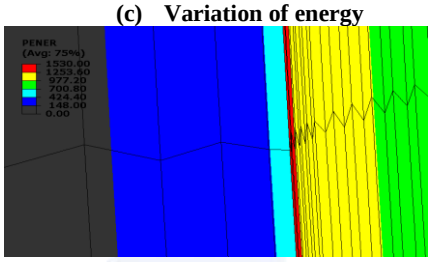

(d) Demarcation of Lc

Fig. 23 Compact tension Specimen (25mm thick, 423oK temperature)

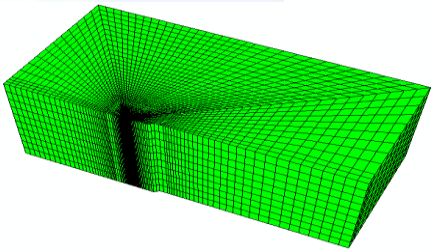

(a) FEM mesh

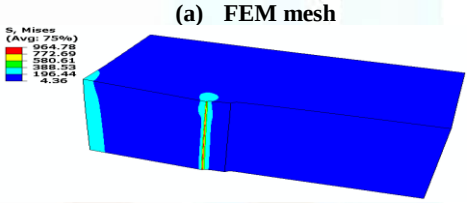

(b) vonMises Stress

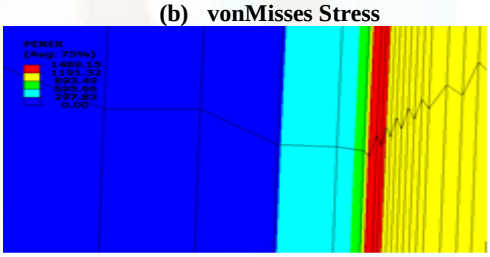

(c) Variation of energy

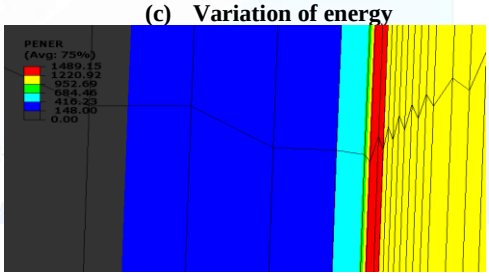

(d) Demarcation of Lc

Fig. 24 Compact tension Specimen (50mm thick, 423oK temperature)

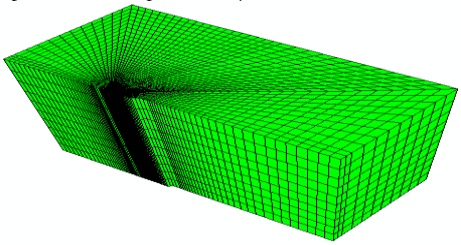

(a) FEM mesh

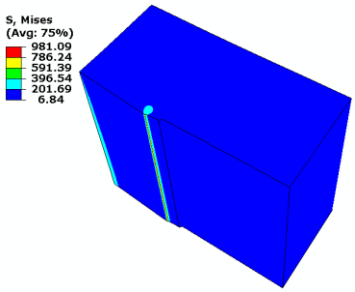

(b) vonMises Stress

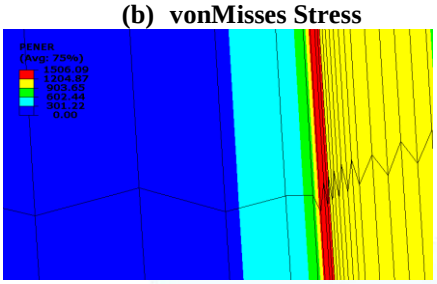

(c) Variation of energy

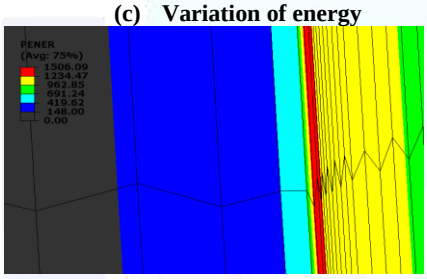

(d) Demarcation of Lc

Fig. 25 Compact tension Specimen (50mm thick, 423oK temperature)

V. Results And Discussion

The research work describes the numerical prediction of characteristic distance and its prediction due to the variation of fracture specimen thickness and due to the change in temperature. The present work uses three-dimensional FEM model of compact tension specimen and tensile property of Armco iron tested at different temperature. The different thicknesses that were considered in the present study are 3.125mm, 6.25mm, 12.5mm, 25mm, 50mm and 100mm thick. Range of temperature that was considered in the present study varies from room temperature (298º K) to 573º K temperatures.

A. Variation of Lc due to fracture specimen thickness

Fig 26 shows the variation of 'characteristic distance' for different temperature of Armco iron across the thickness on a 3.125 mm thick compact tension specimen.

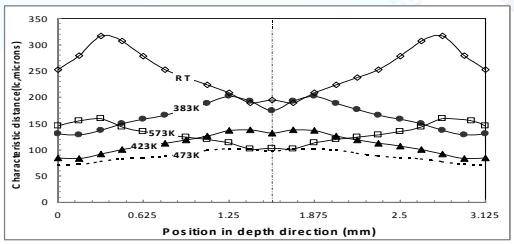

Fig. 26 Variation of lc at various temperatures across the thickness (3.125mm)

The variation of characteristic distance across the thickness can be seen in Fig 26. Characteristic distance value is lower at the two surfaces of fracture specimen whereas it maximizes near the mid thickness of specimen except in case of room temperature results. At room temperature, characteristic distance increases (316 µm) up-to some distance from the surface and thereafter it reduces up-to mid-thickness (195 µm). Considering the magnitude of characteristic distance near the mid thickness of specimen, characteristic distance value decreases from nearly 200 µm up- to 100 µm, with the increase in temperature. This trend is matching even when considering its value at fracture specimen two surfaces except in case of 573º K results. There is also overlapping of different temperature curves, which signifies that the 'characteristic distance' magnitude is same at different temperatures, considering this thickness of fracture specimen.

Fig 27 shows the variation of 'characteristic distance' for different temperature of Armco iron across the thickness on a 6.5 mm thick compact tension specimen.

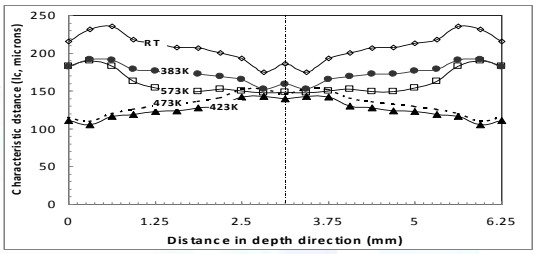

Fig. 27 Variation of lc at various temperatures across the thickness (6.25mm)

The variation of characteristic distance across 6.25mm thick CT specimen can be seen in Fig 25. Characteristic distance value is lower at the two surfaces of fracture specimen in two temperatures (423º K and 473º K) results whereas it maximizes near the mid thickness of specimen. At room temperature, characteristic distance increases up-to some distance from the surface and thereafter it reduces up-to mid-thickness. This trend is same in other two temperatures results also (383º K and 573º K). Considering the magnitude of characteristic distance near the mid thickness of specimen, characteristic distance value decreases from nearly 200µm up-to 140 µm, with the increase in temperature except in case of 573º K. This trend is matching even when considering its value at fracture specimen two surfaces except in case of 573º K results.

Fig 28 shows the variation of 'characteristic distance' for different temperature of Armco iron across the thickness on a 12.5 mm thick compact tension specimen.

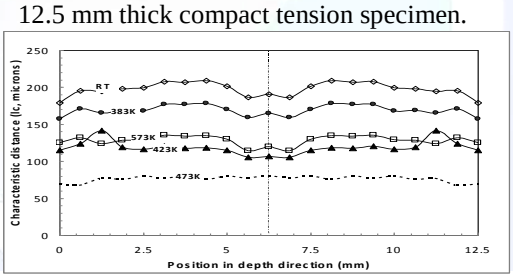

Fig. 28 Variation of lc at various temperatures across the thickness (12.5mm)

The variation of characteristic distance across the 12.5mm thick fracture specimen can be seen in Fig 28. Characteristic distance value is almost same across the thickness of fracture specimen in all the temperatures results. There is a very smooth variation of 'characteristic distance' value across the thickness. Considering the magnitude of 'characteristic distance' near the mid thickness of specimen, characteristic distance value decreases from nearly 200µm up-to 80 µm, with the increase in temperature except in case of 573º K. This trend is matching even when considering its value at fracture specimen two surfaces except in case of 573º K results.

Fig 29 shows the variation of 'characteristic distance' for different temperature of Armco iron across the thickness on a 25 mm thick compact tension specimen.

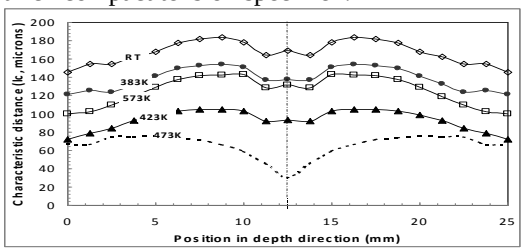

Fig. 29 Variation of lc at various temperatures across the thickness (25mm)

The variation of characteristic distance across the 25mm thick fracture specimen can be seen in Fig 29. Characteristic distance value increases near the mid thickness as compare to its value near the surface. The behaviour is same in all the temperatures results. There is a very smooth variation of 'characteristic distance' value across the thickness. Considering the magnitude of 'characteristic distance' near the mid thickness of specimen, characteristic distance value decreases from nearly 170µm up-to 50 µm, with the increase in temperature except in case of 573º K. This trend is matching even when considering its value at fracture specimen two surfaces except in case of 573º K results.

Fig 30 shows the variation of 'characteristic distance' for different temperature of Armco iron across the thickness on a 50 mm thick compact tension specimen.

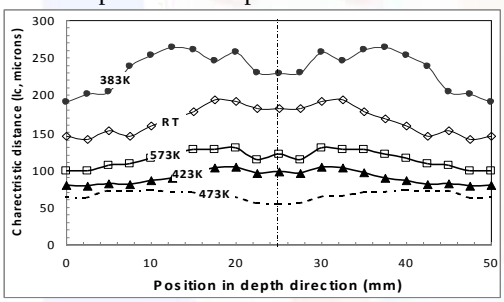

Fig. 30 Variation of lc at various temperatures across the thickness (50mm)

The variation of characteristic distance across the 50mm thick fracture specimen can be seen in Fig 30. Characteristic distance value increases near the mid thickness as compare to its value near the two surfaces. The behaviour is same in all the temperatures results. There is a very smooth variation of 'characteristic distance' value across the thickness. Considering 'characteristic distance' magnitude near mid thickness, there is a slight variation in the characteristic distance value as compared to other thickness of fracture specimen. In 50mm thick specimen, the maximum characteristic distances obtain at 383º K. At mid thickness its value decreases from nearly 250µm to 50 µm. This trend is matching even when considering its value at fracture specimen two surfaces.

Fig 30 shows the variation of 'characteristic distance' for different temperature of Armco iron across the thickness on a 100 mm thick compact tension specimen, characteristic distance value decreases from nearly 140µm up-to 60 µm, with the increase in temperature except in case of 573º K. This trend is matching even when considering its value at fracture specimen two surfaces except in case of 573º K results.

B. Characterization of fracture specimen thickness for valid Lc

In the present study, the variation of magnitude of characteristic distance is found due to the variation of fracture specimen thickness. There are some recommendations available in ASTM 1820 standard for obtaining valid fracture specimen parameter using the fracture specimen geometry. Based on material flow property and toughness of ductile material, ASTM has given the fracture specimen thickness criteria for obtaining valid elastic-plastic fracture parameter. Table VI showed the variation of minimum thickness (B) requirement due to the change of temperature or flow property.

TABLE VI
MINIMUM FRACTURE SPECIMEN THICKNESS REQUIREMENTS FOR VALID RESULTS AS PER ASTM

Tempe-rature	***σ_y (MPa)***	***σ_u (MPa)***	***σ_f (MPa)***	***J_{SZW} (N/mm)***	***$B \geq 25 \frac{J_Q}{\sigma_f}$ (mm)***
RT 298^{O}K	***189***	***296***	***242.5***	***165***	***17***
383^{O}K	***151***	***338***	***244.5***	***230***	***23.52***
423^{O}K	***150***	***385***	***267.5***	***260***	***24.3***
473^{O}K	***148***	***404***	***276***	***290***	***26.27***
573^{O}K	***146***	***404***	***275***	***280***	***25.45***

There are variations in value of characteristic distance across the fracture specimen thickness using the present three-dimensional FEM model. Therefore, to see all the possibility of governing the methodology using 3D model, three possible alternates have been considered in the present study. The maximum value of Lc, minimum value of Lc, and the average Lc value near mid thickness, are the three possible numerical values variation of Lc with thickness are considered in the present study. The variation of Lc with fracture specimen thickness considering Armco iron material tested at different temperatures is given from Fig. 31 to Fig. 35.

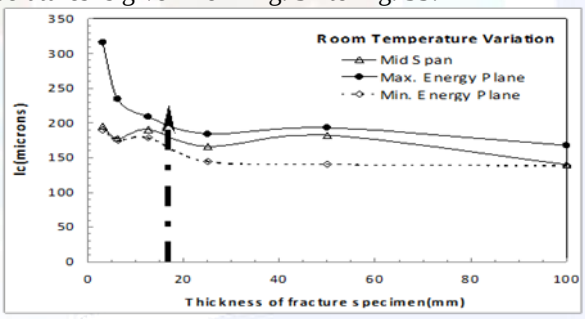

Fig. 31 Variation of Lc with fracture specimen thickness (room temperature)

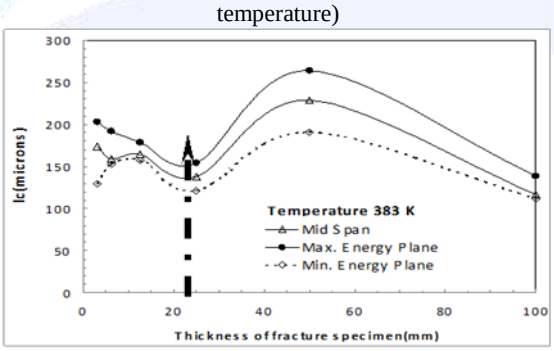

Fig. 32 Variation of Lc with fracture specimen thickness (383OK)

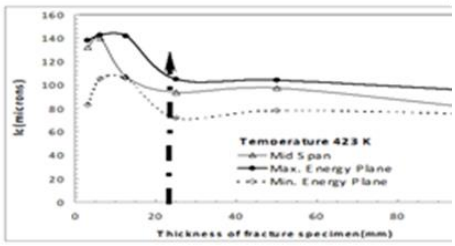

Fig. 33 Variation of Lc with fracture specimen thickness (423OK)

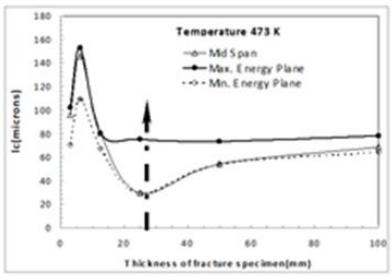

Fig. 34 Variation of Lc with fracture specimen thickness (473OK)

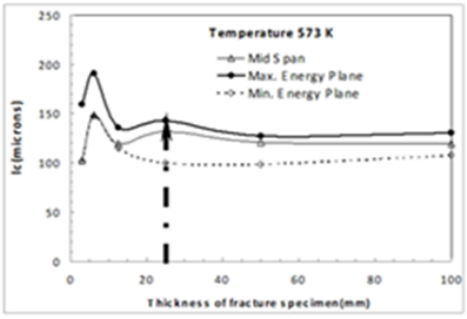

Fig. 35 Variation of Lc with fracture specimen thickness (573OK)

From Fig. 31 to Fig. 35, it can be seen that Lc becomes almost constant after a specified thickness of fracture specimen, except in case of $383^{O}K$ results. The thickness dependency of numerically predicted Lc is similar to other fracture parameter (like J) behaviour with the change of thickness.

C. Variation of Lc due to test temperature fracture specimen thickness

The variation of characteristic distance with the change of temperature can be seen in Fig. 36. The figure has been drawn using the characteristic distance value obtained on 100mm thick specimen, which can be considered as converge Lc value, to be on conservative side. The figures showed the three possible methodologies for the numerical prediction of characteristic distance using three-dimensional FEM model. In all the three results, there is reduction in characteristic distance value when the temperature reaches near $423^{O}K$ to $473^{O}K$, thereafter again increases when reaches at $573^{O}K$.

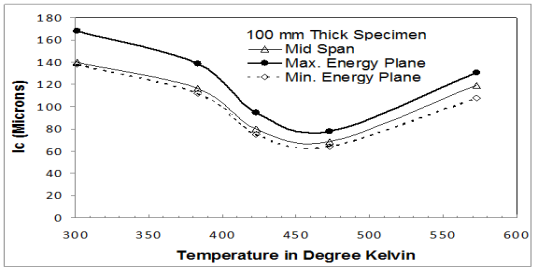

Fig. 36 Variation of 'characteristic distance with temperature

The values of characteristic distance obtained using the lowest characteristic distance across the fracture specimen of characteristic distance from the crack tip, for different temperature can be seen in Table VII.

TABLE VII
CRITICAL AND FRACTURE ENERGY DENSITIES USED

Temperature	*N*	J_{szw} *(N/mm)*	*Lc (mm)*
RT ($298^{O}K$)	*0.29*	*165*	*140*
$383^{O}K$	*0.3*	*230*	*116.5*
$423^{O}K$	*0.41*	*260*	*79.78*
$473^{O}K$	*.48*	*290*	*68.41*
$573^{O}K$	*.38*	*280*	*119.36*

VI. CONCLUSIONS

The present research paper describes the numerical evaluation of characteristic distance fracture parameter using different tensile properties of Armco iron material tested at different temperatures. The numerical prediction methodology of characteristic distance has been tested using three-dimensional FEM model. The work also studied the variation of characteristic distance, due to the change in fracture specimen thickness. Finally the ASTM requirement of fracture specimen thickness criteria is evaluated for the characteristic distance fracture parameter. Following conclusion can be drawn from the present study:

- Characteristic distance varies across the fracture specimen thickness.
- Characteristic distance is dependent on fracture specimen thickness and it converges after a specified thickness of fracture specimen.
- Characteristic distance value is also dependent on the temperature of ductile material.
- In Armco iron material, it is found to decrease with the increase in temperature except at one temperature.

REFERENCES

[1] A. M. Lin'kov," Loss of Stability, Characteristic Length, and Novozhilov–Neuber Criterion in Fracture Mechanics, Institute for Problems in Mechanical Engineering, Russian Academy of Sciences, (2010), pp 61.

[2] B. Yang • S. Shiva, "Crack growth with a part-through process zone in thin plates, Int J Fract, (2010), pp 145-158.

[3] E. E. Kurchakov and G. V. Gavrilov, "Formation of the plastic zone in an anisotropic body with a crack, International Applied Mechanics, Vol. 44, No. 9, (2008).

[4] E. Sarris, P. Papanastasiou, "The influence of the cohesive process zone in hydraulic fracturing modelling, Int J Fract, (2010), pp 33-45.

[5] Franck Vernerey, Wing Kam Liu and Brian Moran, Gregory Olson, "Multi-length scale micromorphic process zone model, Comput Mech, 20 March (2009), pp 433-445.

[6] G.Z.Wang, J.H. Chen and G.H. Liu, "On the characteristic distance and minimum fracture toughness for cleavage fracture in a C-Mn steel, International Journal of Fracture, 16 October (2002), pp 57-76.

[7] H. Hadjab.S & M. Chabaat & J.-Fr. Thimus, "Use of Scanning Electron Microscope and the Non-local Isotropic Damage Model to Investigate Fracture Process Zone in Notched Concrete Beams, Experimental Mechanics, (2007), pp 473-484.

[8] J. Du, M.D. Thouless and A.F. Yee, "Development of a process zone in rubber-modified epoxy polymers, International Journal of Fracture, (1998), pp 271-285.

[9] J. Zhao and X. Zhang, "On the process zone of a quasi-static growing tensile crack with power-law elastic-plastic damage, International Journal of Fracture, 13 September (2000), pp 383-395.

[10] K. Haidar l, G. Pijaudier-Cabot l, J.F. Dub6 2 and A. Loukili, "Correlation between the internal length, the fracture process zone and size effect in model materials, Materials and Structures March (2005) pp 201-210.

[11] K.Y. Volokh, "Characteristic length of damage localization in rubber, Int J Fract, (2010), pp 113–116.

[12] Kaminsky, E. E. Kurchakov, and G. V. Gavrilov, "Influence of tension along a crack on the plastic zone in an anisotropic body, International Applied Mechanics Vol. 46, No. 6, (2010).
[13] L. Jones,S. Maziar Motahari, Mesut Varlioglu, Ulrich Lienert, Joel V. Bernier, Mark Hoffman, Ersan U¨ stu¨ndag," Crack tip process zone domain switching in a soft lead zirconate titanate ceramic, Acta Materialia, 55 (2007), pp 5538–5548.
[14] L.R. Botvina, "Kinetic similarity of fracture processes on various scale levels, International Journal of Fracture, (2004), pp 133-137.
[15] Michael P.Wnuk, "Work of fracture and cohesive stress distribution resulting from triaxiality dependent cohesive zone model, International Journal of Fracture, (2002), pp 29-46.
[16] S. Nakamura, "Finite element analysis of Saint-Venant end effects in micropolar elastic solids, Engineering Computations, 12, (1995), pp 571-587.
[17] Sanjeev Saxena, N. Ramakrishnan, "A comparison of micro, meso and macroscale FEM analysis of ductile fracture in a CT specimen (mode I), Computational Materials Science 39 (2007), pp 1–7.
[18] Sanjeev Saxena, N. Ramakrishnan, B.K. Dutta, "Determination of stretch zone width using FEM, Engineering Fracture Mechanics 76, (2009), pp 911–920.
[19] Sanjeev Saxena, N. Ramakrishnan, J.S. Chouhan," Establishing methodology to predict fracture behaviour of piping components by numerically predicting specimen fracture data using tensile specimen test, Engineering Fracture Mechanics 77 (2010), pp 1058–1072.
[20] V. Kashtanov, Yu. V. Petrov, N. Pugno, A. Carpinteri, "Dynamic fracture as a process of nonlinear damage wave propagation, Int J Fract, (2008), pp 227-240.
[21] WU Yan-qing, Zhang Ke-shi, "crack propagation in polycrystalline elastic-viscoplastic materials using cohesive zone models, Applied Mathematics and Mechanics, (2006), pp 509–518.
[22] Xiaozhi Hu, Kai Duan, "Size effect: Influence of proximity of fracture process zone to specimen boundary, Engineering Fracture Mechanics, (2007), pp 1093-1100.
[23] Ye Zhiming, "The damage process zone characteristics at crack tip in concrete, Applied Mathematics and Mechanics, (1996), Vol. 19, No. 1.